Du *et al. J. Mater. Inf.* **2025**, *5*, 10
DOI: 10.20517/jmi.2024.68

Journal of Materials Informatics

Research Article

Open Access

Towards mechanical performance paradox and behind thermo-kinetic origins of aluminum alloys with additional solutes (X = Mg, Cu and Si) from atomistic simulations

Jinglian Du[1,*], Yu Liu[1], Caisi Zhao[1], Haotian Xue[1], Kangxu Gao[1], Xiao Fang[1], Kexing Song[2], Feng Liu[1,3,*]

[1]State Key Laboratory of Solidification Processing, Northwestern Polytechnical University, Xi'an 710072, Shaanxi, China.
[2]Henan Academy of Sciences, Zhengzhou 450046, Henan, China.
[3]Analytical & Testing Center, Northwestern Polytechnical University, Xi'an 710072, Shaanxi, China.

[*]**Correspondence to:** Prof. Jinglian Du, Prof. Feng Liu, State Key Laboratory of Solidification Processing, Northwestern Polytechnical University, No. 127, Youyi West Road, Xi'an 710072, Shaanxi, China. E-mail: dujl666@nwpu.edu.cn; E-mail: liufeng@nwpu.edu.cn

How to cite this article: Du, J.; Liu, Y.; Zhao, C.; Xue, H.; Gao, K.; Fang, X.; Song, K.; Liu, F. Towards mechanical performance paradox and behind thermo-kinetic origins of aluminum alloys with additional solutes (X = Mg, Cu and Si) from atomistic simulations. *J. Mater. Inf.* **2025**, *5*, 10. https://dx.doi.org/10.20517/jmi.2024.68

Received: 31 Oct 2024 **First Decision:** 2 Jan 2025 **Revised:** 21 Jan 2025 **Accepted:** 7 Feb 2025 **Published:** 13 Feb 2025

Academic Editors: Xiao-Dong Xiang, Qian Li, Xiang-Dong Ding **Copy Editor:** Pei-Yun Wang **Production Editor:** Pei-Yun Wang

Abstract

Dislocation glide and/or deformation twinning, which can be uniformly described as the kinetic behaviors of atoms driven by thermodynamics, play important roles in dominating mechanical performance and strength-ductility paradox of metallic alloys. In this work, the physical origins behind the mechanical performance paradox are investigated in light of thermo-kinetic synergy upon materials processing. Combining the classical dislocation theories with common strengthening mechanisms, the quantitative connections among yield strength, plastic strain and dislocation density are bridged by the driving force and energy barrier of dislocation motion. The FCC-Al and Al alloys with Mg, Cu and Si solutes are studied as typical representatives by performing molecular dynamics (MD) simulations to analyze the tensile behaviors. It turns out that the thermo-kinetic synergy is responsible for the strength-ductility exclusive behaviors. The yield strength and flow stress are enhanced with Mg, Cu and Si solutes adding in FCC-Al, due to the increased interactions between dislocations and solute atoms. All the Mg, Cu and Si solutes can benefit the mechanical responses of Al alloys. Increasing Mg content enhances the driving force and yield stress of Al-Mg alloys, but reduces the energy barrier and plastic strain. The solute Si addition can further increase the driving force and yield stress, but decrease the energy barrier and plastic strain of Al-Mg-Si alloys. Our

investigation provides an innovative viewpoint for understanding the mechanical performance paradox of metallic alloys, and offers insightful guidance for designing advanced Al alloys with good mechanical performance.

Keywords: Mechanical performance paradox, deformation behaviors, thermo-kinetic synergy, dislocation motion, aluminum alloys

INTRODUCTION

As one of the lightweight metallic materials, aluminum (Al) alloys have widespread applications in aerospace, construction, and automotive manufacturing industries due to their outstanding performance including high specific strength, good processing formability and environmental friendliness[1-3]. For the engineering requirements of Al alloys used in the components with large thermo-mechanical loads, high strength is usually needed to ensure stability and safety, whereas, in the components with complex shapes such as architectural decorative parts, good ductility is required to satisfy the processing techniques[4-6]. However, the strength and ductility of Al alloys exhibit exclusive behaviors. This mechanical performance paradox is known as the strength enhancement generally as a sacrifice of ductility, and vice versa[7-12], which is attributed to the microstructural characteristics and deformation mechanisms. In practical applications, such as aircraft envelopes and automobile body frames, both initial yield strength and uniform elongation are important for Al alloys to withstand impact loads and avoid component breakage[5-8]. Therefore, achieving an ideal strength-ductility match becomes both scientifically significant and technologically important for the development of advanced Al alloys with good comprehensive mechanical performance, which depends on clarifying the physical origins behind the above performance paradox and breaking through the primitive trade-off correlation between strength and ductility.

During the past decades, much more efforts from both theoretical and experimental works[13-19] have been devoted to understanding the mechanical performance paradox in terms of the strengthening/toughening mechanisms and microstructure-property correlations, aiming to find the influential factors contributing to an ideal strength and ductility match by methods such as adjusting the additional solutes and/or optimizing the thermomechanical processing parameters of Al alloys[20-26]. Nevertheless, the underlying mechanism behind the above mechanical performance paradox remains an unsolved mystery, which impedes the development of higher-performing Al alloys. In general, the mechanical performance of materials can be reflected by loading the microstructure, where the interactions between dislocations and different kinds of crystalline defects (such as solutes/vacancies, atomic clusters, other different kinds of dislocations, grain/phase boundary and the second phase precipitated in the alloy system) play dominant roles in controlling the strength and ductility of Al alloys[27-32]. Plastic deformation is primarily governed by dislocation glide and deformation twinning[2,33-36], which is actually a kinetic process of atoms or atomic groups driven by thermodynamics[37,38]. Therefore, it is believed to be a pertinent viewpoint to understand the above mechanical performance paradox in light of the thermo-kinetic synergy upon materials processing. With this respect, the thermo-kinetic partition and/or generalized stability[37,39] was proposed from the connectivity and correlation between thermodynamics and kinetics for phase transition and deformation[12,18,40-44]. Its applications have been verified in the reverse austenite transition by interface movement and the plastic deformation by dislocation motion in different metals such as magnesium alloys and alloy steels[45,46]. By integrating this concept with respect to nucleation and growth processes of the microstructure formation and deformation, it is found that alloys with high strength and high ductility correspond to the large driving force and large energy barrier[12,45]. However, these previous studies are mostly qualitative descriptions with unknowing the specific values of generalized stability from relevant thermo-kinetic calculations. Thus, everlasting investigations on the thermodynamics and kinetics of dislocation behaviors are required to understand the above mechanical performance paradox in terms of

establishing the quantitative strength and ductility models.

In the present work, the exclusive behaviors of strength and ductility, along with the physical origins, of FCC-Al and Al alloys are investigated from the viewpoint of thermo-kinetic synergy upon materials processing in combination with classical dislocation theories and atomistic simulations. Theoretical models for quantitative correlations between the driving force and flow stress, together with that between the plastic strain and effective energy barrier for dislocation motion, are established. The tensile behaviors and mechanical responses of FCC-Al and Al alloys with additional solutes Mg, Cu and Si are analyzed by performing molecular dynamics (MD) simulations. The generalized stability concerning the thermo-kinetic calculations on driving force and energy barrier in terms of dislocation density are obtained based on the common strengthening-toughening mechanisms of Al alloys. Accordingly, the effects of additional Mg, Cu and Si solutes on the mechanical behaviors of Al alloys are discussed for validation of the established quantitative models. Afterwards, the thermo-kinetic origins behind the strength-ductility exclusive behaviors of Al alloys are analyzed, along with the prospect of the current thermo-kinetic models applied in design higher-performing alloys.

MATERIALS AND METHODS

Thermo-kinetic description for dislocation behaviors

Following the classical dislocation theories, the effective driving force (ΔG or $\Delta\sigma$) for dislocation motion during irreversible deformation is regarded as the difference between the applied stress σ_f (or flow stress) and the glide resistance σ_{res} (usually induced by different crystalline defects including solute atoms, dislocations, grain/phase boundaries, precipitates, *etc.*) derived from interactions between these defects and dislocations[47-50], as given by:

$$\Delta G = \sigma_f - \sigma_{res} \tag{1}$$

In general, the dislocation glide resistance[47,51] can be expressed as:

$$\sigma_{res} = \Delta\sigma_{ss} + \Delta\sigma_{gb} + \left(\Delta\sigma_{dis}^n + \Delta\sigma_{pre}^n\right)^{1/n} \tag{2}$$

where the exponent n varies between 1 and 2, especially $n = 1$ when the weak particles are dominant, and $n = 2$ corresponds to strong obstacles from the precipitates (i.e., the strength of precipitate particles comparable to the dislocation glide resistance). $\Delta\sigma_{ss}$ denotes the dislocation glide resistance contributed from solid solution atoms[52], which can be acquired from:

$$\Delta\sigma_{ss} = \sum_{i=1}^{m} k_i C_i^{2/3} \tag{3}$$

where m is the number of solute i, k_i is the temperature-dependent factor of solute i, and C_i is the mole fraction of solute i. $\Delta\sigma_{gb}$ denotes the glide resistance contributed from grain boundaries[53], which can be estimated from:

$$\Delta\sigma_{gb} = K d^{-0.5} \tag{4}$$

where K is the Hall-Petch coefficient, and d is the mean grain size. $\Delta\sigma_{dis}$ denotes the dislocation glide resistance contributed by interaction among dislocations[33], which can be evaluated from:

$$\Delta\sigma_{dis} = M\alpha b\mu\rho_t^{0.5} \tag{5}$$

where M is the Taylor factor, α is the numerical factor with respect to temperature and strain rate, b is the Burgers vector, μ is the shear modulus, and ρ_t is the total dislocation density. $\Delta\sigma_{pre}$ denotes the glide resistance contributed from the second phase precipitated in alloy system[54], which can be predicted from:

$$\Delta\sigma_{pre} = MF/bl \tag{6}$$

where F is the maximum force interacted between dislocations and precipitates, and l is the effective distance between two precipitates. In general, a large glide resistance σ_{res} in Equation (1) implies a more difficult deformation to occur, and a more contribution from thermodynamics than kinetics. This is reflected by a smaller activation volume or thermo-kinetic partition[37], which corresponds to a weaker work hardening effect.

In parallel, the effective energy barrier (Q) or activation energy for dislocation motion upon deformation can be obtained in combination with the Orowan equation and dislocation kinetics[50,55-57], as given by:

$$\varepsilon = \frac{bv_0\rho_m L_{eff} t}{M}\exp\left(-\frac{Q}{RT}\right) \tag{7}$$

$$\varepsilon = bl\rho_m/M \quad (\text{or} \quad \dot{\varepsilon} = bv\rho_m/M) \tag{7a}$$

$$v = v_0 L_{eff}\exp\left(-Q/RT\right) \tag{7b}$$

where ε is the plastic strain, v_0 is the attack frequency for thermal fluctuation, ρ_m is the mobile dislocation density, L_{eff} is the effective separation of dislocation slip, $\dot{\varepsilon}$ is the strain rate, R is the gas constant, and T is the temperature.

Following the thermo-kinetic correlation[38], the effective energy barrier at any transient state during dislocation evolution after yielding can be obtained in light of the activation volume and stress increment, which corresponds to the activation energy in terms of the driving force variation $\Delta\sigma$[58,59], as expressed by:

$$Q = Q_0 - V^*\Delta\sigma \tag{8}$$

$$Q_0 = Q_y + V^*\Delta\sigma_y \tag{8a}$$

where Q_0 is the effective activation energy without applied stress driven ($\Delta\sigma = 0$), V^* is the activation volume. Especially, the effect activation energy at the yield point is written as Equation (8a), where Q_y and $\Delta\sigma_y$ denotes the corresponding energy barrier and driving force, respectively. Such derivation is analogous to the simplified version for the Olson-Cohen model[49]. Following Equation (8), the activation volume is written as:

$$V^* = \frac{Q - Q_y}{\Delta\sigma_y - \Delta\sigma} \tag{9a}$$

$$V^* = dQ/d\Delta\sigma \tag{9b}$$

which is denoted by the ratio between energy barrier and driving force, and thus named as the thermo-kinetic partition for dislocation motion.

In principle, the dislocation nucleation is mostly initiated at the yield point upon deformation. By taking the yield point as the reference state and normalizing the numerator and denominator via Q_y and $\Delta\sigma_y$ in the right hand of Equation (9), there is:

$$V^* \frac{\Delta\sigma_y}{Q_y} = \frac{Q/Q_y - 1}{1 - \Delta\sigma/\Delta\sigma_y} \tag{10}$$

For convenience, a dimensionless parameter was introduced as generalized stability Δ_{gs}[38,39] to describe the durability of dislocation motion during irreversible deformation, i.e.,

$$\Delta_{gs} = \frac{Q}{Q_y} - \frac{\Delta\sigma}{\Delta\sigma_y} \tag{11}$$

Apparently, the value of generalized stability is zero at the yield point. An increased ductility for uniform elongation or plastic deformation (with a smaller activation volume or thermo-kinetic partition) should correspond to the dislocation behaviors with continuously decreased generalized stability[37]. As such, the generalized stability and the thermo-kinetic partition, which can be used to quantitatively describe the system energy accumulation or dissipation speed of irreversible deformation, were introduced to describe the persistence of dislocation motion. In general, the dislocation evolution is accompanied by an enhanced driving force and reduced energy barrier[38], and thus consecutively reduced generalized stability, which derives from the continuously increased thermo-kinetic partition reflecting the continuously increased ductility. For any transient state during deformation, by comparing series dislocation motion processes, a higher generalized stability reflects both a lower sustainability and a more stable status that possesses greater potential to continue the uniform deformation, i.e., better ductility. The more contribution from dislocation nucleation and/or multiplication (larger ρ_t), the higher the driving force and/or the strength, while the more contribution from dislocation slip (larger ρ_m), the higher the generalized stability and/or the ductility. Thus, the generalized stability and/or thermo-kinetic partition can be used to reflect the ductility.

By considering the glide resistance from solid solution, grain boundary and dislocations in Equations (1) and (2), i.e., the dislocation-solute along with dislocation-grain boundary and dislocation-dislocation interactions, the alloy strength with respect to the driving force for dislocation motion can be obtained from:

$$\Delta G = \sigma_f - \left(\sum_{i=1}^{m} b_i C_i^{0.5} + K d^{-0.5} + M \alpha \mu b \rho_t^{0.5} \right) \tag{12}$$

Meanwhile, the plastic strain associated with the energy barrier for dislocation motion can be acquired from:

$$\varepsilon = k \cdot \exp\left(-Q/RT \right) \tag{13}$$

$$k = \frac{b v_0 \rho_m L_{eff} t}{M} \tag{13a}$$

As such, the critical thermo-kinetic parameters including driving force and energy barrier during irreversible deformation can be obtained, with inputs being listed in Table 1. Accordingly, the underlying physical origins behind the exclusive behaviors of strength and ductility can be understood from the

Table 1. Relevant inputs for determination of the thermo-kinetic parameters for dislocation motion upon deformation of FCC-Al and Al alloys, including the Taylor factor, the Taylor hardening coefficient, the shear modulus, the Burgers vector, the solid solution constant, the gas constant, and the Hall-Petch coefficient

Parameters	Value	Ref.
Taylor factor, M	3.06	[32,47]
Taylor hardening coefficient, α	0.3	[32,33]
Shear modulus of FCC-Al, μ	27 GPa	[26]
Burgers vector of FCC-Al, b	0.286 nm	[32,47]
Solid-solution constant of Mg, k_{Mg}	29.0 MPa/wt.%$^{2/3}$	[52]
Solid-solution constant of Si, k_{Si}	66.3 MPa/wt.%$^{2/3}$	[52]
Gas constant, R	8.314 J/(mol·K)	[98]
Hall-Petch coefficient, K	0.12 MPa/m$^{1/2}$	[78]

synergistic effects of thermodynamics and kinetics upon materials processing.

Computational methods

All the MD simulations herein were performed by the Large-scale Atomic/Molecular Parallel Simulator (LAMMPS) package[60]. The modified embedded atom method (MEAM) potential developed by Jelinek *et al.* was employed[61]. This potential was validated to reasonably capture the defects' structure and mechanical properties[62,63], including the elastic moduli, stacking fault energy (SFE), and formation energies of different defects in Al alloys; thus, it has been widely used to investigate the deformation mechanism and mechanical performances of alloys[64-67], such as the mechanical responses of nanocrystalline Al under uniaxial loading conditions, the formation of dislocations on the second-order pyramidal planes, and the tensile stress-strain behaviors of high entropy alloys. The three-dimensional periodic boundary conditions[68] were employed during the MD simulations. The energy minimization was carried out by the conjugate gradient method[69] to acquire the equilibrium configuration. Before exerting the stretching strain, it was relaxed for 300 ps in the NPT ensemble[68] to stabilize the system at the prescribed temperature of 300 K. The atomic coordination was updated using the Velocity Verlet algorithm[69] with a time step of 0.05 ps. After attaining equilibrium, the alloy samples were stretched at a constant strain rate of 1×10^8 s^{-1} along the z axis, i.e., <001> direction of the simulation box, while the x and y axes maintained at pressure of 0 Pa.

The Open Visualization Tool (OVITO)[70] offers post-processing abilities to obtain snapshots at transient loading moments and to visualize the stretching configurations of the simulated alloy samples. Thus, the results obtained from MD simulations were visualized by the OVITO package to capture and trace the variations in dislocation distributions and atomic configurations by the dislocation extraction algorithm (DXA) techniques[71]. The supercell size for the MD simulations is set as $32.4 \times 32.4 \times 32.4$ nm^3, i.e., $80a \times 80a \times 80a$ with $a = 0.405$ nm being the lattice parameter of FCC-Al. Taking binary Al-Mg alloy as an example, Figure 1A shows the alloy samples for the present tensile simulation. Figure 1B presents the atomic types of constitutional elements with the red and blue spheres denoting the matrix Al atoms and the solute Mg atoms, respectively. Figure 1C represents the structural types with the green, red, blue and light grey colors denoting the FCC structure, the BCC structure, the HCP structure and the other structure (including the atoms at grain boundaries and/or interstices). Figure 1D and E presents the distribution of crystalline defects such as the grain boundaries and dislocations, where the blue, pink, green, yellow, cyan and red lines represent the <110>/2, <110>1/6, <112>1/6, <100>/3, <111>/3 and other types of dislocations, respectively. The corresponding simulation box contains ~2 million atoms with six randomly oriented crystalline grains (mean size of ~22 nm) in the alloy system.

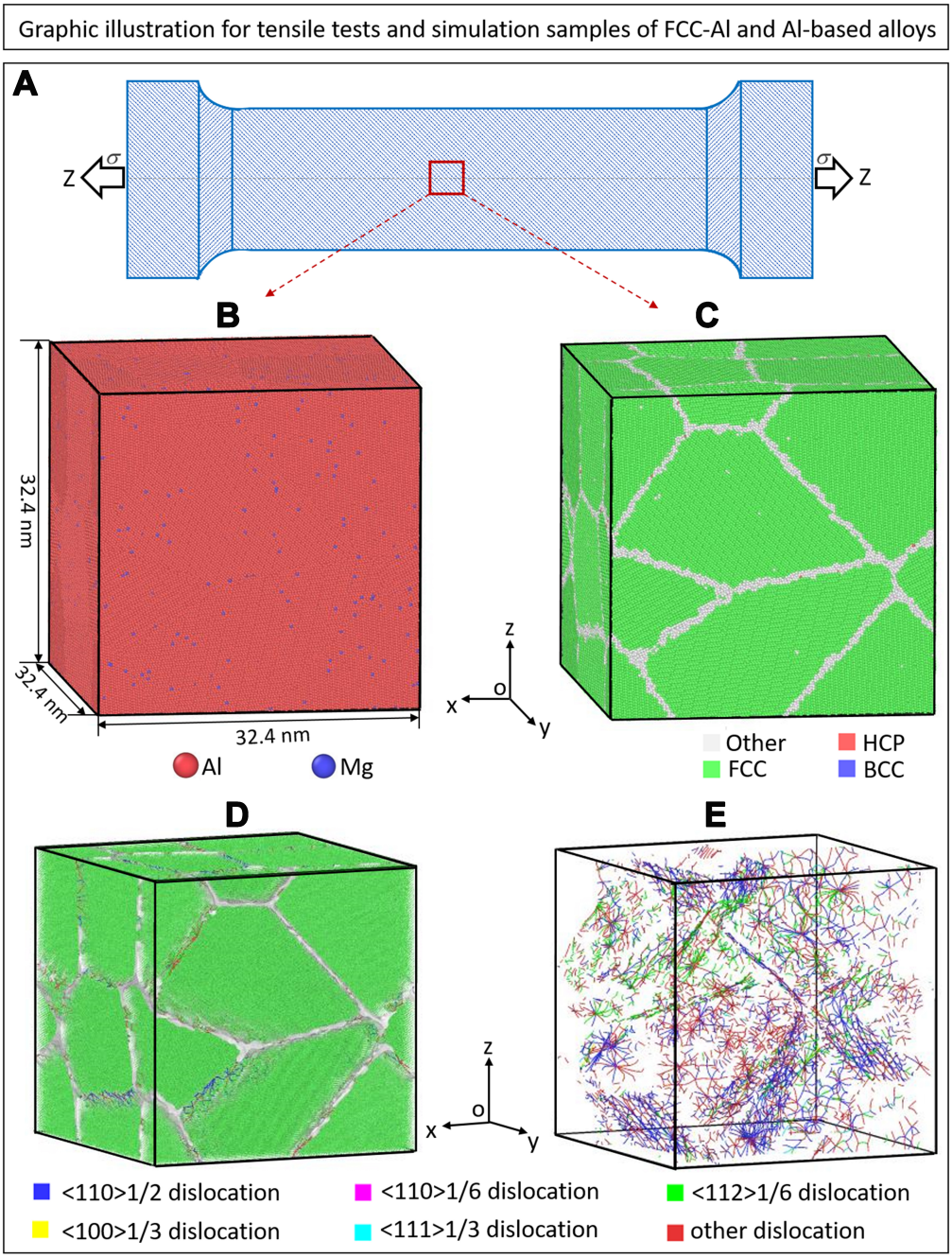

Figure 1. Schematic illustration for the tensile tests of (A) FCC-Al and Al-Mg alloy samples with average grain size of 22 nm, where the atoms in the structural model are described in terms of (B) the atomic type of constitutional elements, (C) the common-neighbor analysis, (D) the defects presentation, and (E) the dislocation distribution. Note that the red spheres and blue spheres in (B) represent the matrix Al atoms and solute Mg atoms, respectively. The regions with green, red, blue and light grey colors in (C) represent the FCC structure, the HCP structure, the BCC structure and the other structure (including atoms at the grain boundaries and/or interstices), respectively. The blue, pink, green, yellow, cyan, and red lines in (D) and (E) represent the <110>/2, <110>1/6, <112>1/6, <100>/3, <111>/3, and other type of dislocation, respectively.

RESULTS AND DISCUSSION

Tensile behaviors of FCC-Al and Al-based alloys

The tensile stress-strain curves of FCC-Al and its alloys were obtained to investigate the Mg, Cu and Si

alloying effects on their mechanical behaviors. The results are shown in Figure 2, where insert maps present the according variations of mobile dislocation density. Specifically, the tensile curves of FCC-Al along with binary Al-0.78at.%Mg and Al-0.78at.%Cu alloys are presented in Figure 2A. It is found that the stress increases linearly with the strain at the first stage (e.g., strain < 0.04 for FCC-Al), which corresponds to the elastic deformation before the yield point. Subsequently, the tensile curves become steady at the second stage (e.g., strain within 0.04-0.10 scope for FCC-Al) corresponding to the uniform plastic deformation. The flow stress reaches a near-constant value in this stage, where the dislocation multiplication and annihilation are balanced with each other, as the evolution of dislocation distribution is reflected in Figure 3. Such variations in the tensile stress-strain curves are in agreement with that reported in previous work[72], where analogous tensile behaviors of Al alloys were observed. The addition of both Mg and Cu solutes enhances the yield strength and flow stress of Al alloys due to the increased glide resistance from the interactions between dislocations and these solute atoms in the systems. As reflected by the tensile curves in Figure 2A, the yield strength and flow stress (at strain $\varepsilon = 0.1$) increase to 6.25% and 11.5% for the Al-0.78at.%Cu alloy, respectively, while to 6.77% and 11.5% for the Al-0.78at.%Mg alloy in comparison with pure Al. Thus, the influences on mechanical responses of the 0.78at.%Mg solute (red curve) are more apparent than that of the 0.78at.%Cu solute (blue curve) added in FCC-Al (black curve).

Figure 2B shows the tensile curves of binary Al-Mg alloys with different solute Mg contents. It is observed that the yield strength and flow stress increase gradually with the Mg solutes in FCC-Al. The tensile curves of ternary Al-Mg-Si alloys with different Mg and Si solute contents are shown in Figure 2C. Consistent with FCC-Al, Al-Mg and Al-Cu alloys, the tensile curves of the Al-Mg-Si alloys exhibit analogous variation trends, which are accompanied by the gradually increased mobile dislocation density from the yield point to the second stage. Notably, the Cu, Mg and Si solutes added in FCC-Al cause high flow stress and large mobile dislocation density. With increasing contents of Mg and Si solutes, the lattice resistance increases at the early strain stage where the dislocations are relatively scarce, accompanied by increased strength. These predicted results are in agreement with the experimental findings[73-75] that alloying Mg, Cu and Si solutes with FCC-Al can strengthen the Al alloys. The resistance of dislocation motion is enhanced via the increased interactions between dislocations and these solute Mg, Cu and Si atoms added in FCC-Al.

Note that an apparent problem on the tensile behaviors determined from the MD simulations is the over-prediction for flow stress by a larger factor than that from experimental results[76]. Such distinctions are attributed primarily to the following reasons. (i) The strain rate: the mechanical behaviors as reflected by yield strength and/or flow stress of metallic alloy is sensitive to strain rate, and in general, a higher strain rate condition corresponds to a larger flow stress[77]. The tensile tests in practical cases are usually performed at quasi-static conditions with an initial strain rate of 10^{-4}-10^{-3} s^{-1}[45], which is several orders of magnitude smaller than that (e.g., 10^{8}-10^{9} s^{-1}) used in the MD simulations. The high strain rate of 1×10^{8} s^{-1} used in the present MD simulations results in the predicted flow stress of Al alloys higher than experimental values. (ii) The grain size: the MD simulations mostly focus on the nanocrystals, while the grain size of Al alloys is usually at the micrometer scale in practical situations[76,78]. For instance, the mean grain size for the present MD simulations is set as ~22 nm, which is considerably smaller than the measured grain size of Al alloys at micrometer scale in experiments, e.g., 1.07-150 μm reported in the literature[45,79]. Following the Hall-Petch correlation, such distinctions in grain size lead to the predicted stress higher than the experimental value. With this respect, it was reported that the strength from grain boundary is generally negligible, and for medium-to-high strength alloys, the grain boundary strengthening is swamped by other strengthening modes[80], unless ultra-high cooling rates result in the nano-size grains[81]. (iii) The initial dislocations: there are initial dislocations mostly in practical alloy systems. The yielding is governed by multiplication of the existing dislocations in practical cases, which needs a smaller stress than that of the ideal crystals without

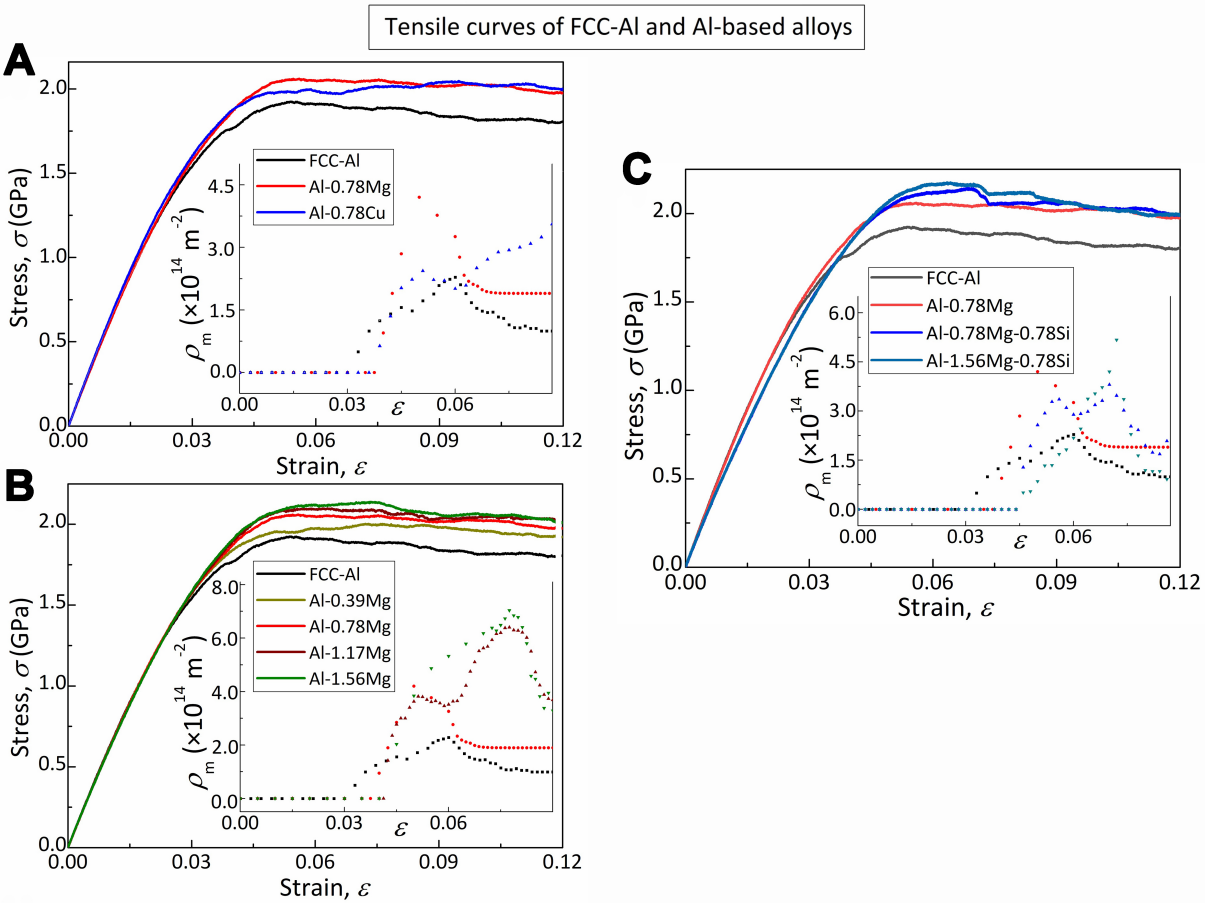

Figure 2. The stress-strain curves of FCC-Al and Al alloys. (A) Tensile curves of binary Al-0.78at.%X alloy with additional Mg and Cu solutes; (B) Tensile curves of binary Al-Mg alloys with different Mg solute contents; (C) Tensile curves of ternary Al-Mg-Si alloys with different solutes Mg and Si contents. Insert map shows the corresponding variations of mobile dislocation density upon tensile deformation. The averaged values of three tests were taken for plotting the tensile curves.

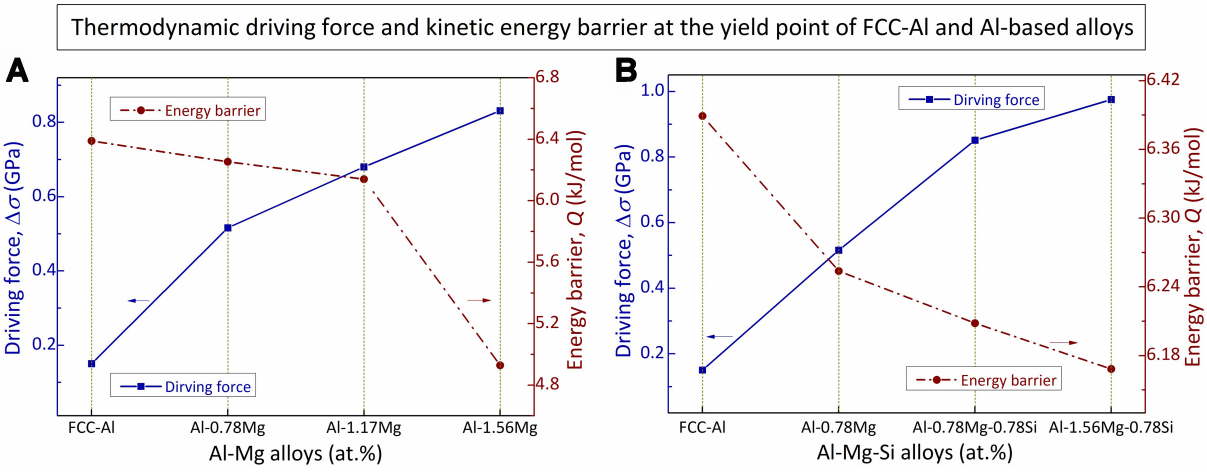

Figure 3. Thermo-kinetic variations of FCC-Al and Al alloys at the yield point. The calculated values of thermodynamic driving force and kinetic energy barrier at the yield point of (A) binary Al-Mg alloys and (B) ternary Al-Mg-Si alloys with different solutes Mg and Si contents, respectively.

initial dislocations in the present MD simulations.

Thermo-kinetic variations upon tensile deformation

Based on Equations (12) and (13) introduced in terms of thermo-kinetic synergy, the driving force and energy barrier for dislocation motion upon deformation of FCC-Al and Al alloys were obtained. Figure 3 shows the variation of driving force and energy barrier for dislocation motion of FCC-Al and Al alloys at the yielding point. Specifically, the thermo-kinetic variation in binary Al-Mg alloys with respect to different Mg contents is presented in Figure 3A, while that in ternary Al-Mg-Si alloys with respect to different contents of Mg and Si solutes in Figure 3B. It is observed that the increase of thermodynamic driving force is accompanied by the decrease of the kinetic energy barrier for dislocation motion. Such intrinsic thermo-kinetic trade-off correlations are exhibited in both binary Al-Mg alloys and ternary Al-Mg-Si alloys. At the yield point, the driving force is enhanced but the energy barrier is reduced with increasing contents of Mg and Si solutes in FCC-Al. For example, the driving force (energy barrier) for dislocation motion at the yield point enhances (reduces) from 0.15 GPa (6.39 kJ/mol) for FCC-Al to 0.52 GPa (6.25 kJ/mol) for Al-0.78at.%Mg alloy and to 0.83 GPa (4.93 kJ/mol) for Al-1.56at.%Mg alloys. Further addition of 0.78at.%Si in Al-Mg alloys enhances (reduces) the driving force to 0.85 GPa (6.21 kJ/mol) for Al-0.78Mg-0.78Si alloy and to 0.98 GPa (6.17 kJ/mol) for Al-1.56Mg-0.78Si alloys.

The irreversible deformation governed by dislocation behaviors corresponds to a process featured by the enhanced driving force and reduced energy barrier from the yielding to the necking point[38]. From the MD simulations, the dislocation nucleation and slip at the yield point induces abrupt reorientation of the crystal lattice caused by strain, along with the enhanced flow stress and driving force for dislocation motion in FCC-Al and Al alloys. After yielding, the mobile dislocation density increases with dislocation propagation in the alloy systems, resulting in an increased energy barrier. Such a phenomenon was also observed in previous MD simulations on the deformation of tantalum crystals[76]. In addition, the yield point is postponed with the Mg, Cu and Si solutes added in FCC-Al. For instance, the strain at the yield point was delayed from 0.054 for FCC-Al to 0.06 for Al-0.78Mg alloys and to 0.09 for Al-0.78Cu alloys. The addition of 0.78at.%Si in the Al-Mg alloys can further postpone the yield point to 0.068 for Al-0.78Mg-0.78Si alloy and to 0.064 for Al-1.56Mg-0.78Si alloy. With increasing contents of Mg and Si solutes, the driving force at the yield point enhances, while the energy barrier reduces. This confirms the trade-off correlation between the driving force and energy barrier for dislocation motion in these Al alloys. The underlying reason is attributed to the Mg and Si solutes restricting the mobile dislocations in the α-Al matrix, which induces enhancement of external stress to overcome the increased glide resistance with respect to the reduced mobile dislocations in the alloy systems.

Such thermo-kinetic variations are in accordance with the experimental findings[74,75], where the additional solutes resulting in the hardening effects correspond to an enhanced driving force for dislocation motion, while the exhaustion and/or trapping of mobile dislocations induces the decreased mobile dislocations in terms of the reduced energy barrier. This signifies the trade-off correlation between thermodynamic driving force and kinetic energy barrier for dislocation motion of Al-based alloys. In general, a larger dislocation motion velocity and total dislocation density are related to a small mobile dislocation density due to an enough high rate for dislocation exhaustion. The simultaneous increase of total dislocation density and decrease of mobile dislocation density corresponds to an enhanced driving force and reduced energy barrier for dislocation motion. Thus, the work hardening stage requires continuously enhanced applied stress, which favors dislocation nucleation rather than dislocation glide, as reflected by the high strength but low ductility.

Thermo-kinetic origins behind the mechanical performances paradox

According to the above thermo-kinetic analysis, the generalized stability of FCC-Al and Al alloys is obtained to estimate the dynamic stability during plastic deformation. Figure 4 shows stress at the yield point and generalized stability at the strain point of 0.1 for FCC-Al and Al alloys with different solutes X = Mg, Cu and Si. The predicted stress of 1.92 GPa at the yield point for FCC-Al agrees with that of 1.6-2.1 GPa reported in the literature from MD simulations[82-84], which confirms the reliability of the present MD simulations. The slight differences among these predicted values derived from the input settings of initial configurations and testing conditions in MD simulations, including the box size, strain rate, potentials, *etc.* The flow stress and yield strength are enhanced after adding Mg, Cu and Si solutes in FCC-Al. In contrast, the generalized stability varies reversely; i.e., the value of Δ_{gs} decreases with addition of the Mg, Cu and Si solutes. For instance, with 0.78at.% Mg and Cu solutes adding in FCC-Al, the yield strength enhances from 1.92 to 2.05 and 2.04 GPa, respectively, whereas the generalized stability decreases from 0.99 for FCC-Al to 0.71 and 0.61 for Al-0.78at.%Mg and Al-0.78at.%Cu alloys, respectively.

With increasing contents of Mg solute in FCC-Al, the increased yield stress of Al-Mg alloys is accompanied by decreased generalized stability. For example, with Mg solute rising from 0.78at.% to 1.56at.%, the yield stress of the Al-Mg alloys grows from 2.05 to 2.13 GPa, while the generalized stability (at ε = 0.1) decreases from 0.71 to 0.54. Further addition of 0.78at.%Si solute enhances (reduces) the yield stress (generalized stability) to 2.14 GPa (0.43) for Al-0.78Mg-0.78Si alloys. The addition of 0.78at.%Mg in Al-0.78Mg-0.78Si alloys further enhances the yield stress to 2.17 GPa but decreases the generalized stability to 0.39 for Al-1.56Mg-0.78Si alloys. Specifically, the generalized stability increases from 0 at the yield point to 0.99 at the strain point of ε = 0.1 for FCC-Al. At the same strain point, the Al alloy (X = Mg, Cu and Si) systems show more stable states and easier to sustain more continuous dislocation evolution than the FCC-Al. Within the same strain scope (e.g., 0.05-0.1), the FCC-Al possesses lower flow stress and higher generalized stability in comparison with the Al alloys with Mg, Cu and Si solutes studied in the present work.

Apparently, an increased strain during irreversible deformation corresponds to a more sustainable process of dislocation evolution, which favors lower dynamic stability. Although different trends of generalized stability vary between experiments and MD simulations, the tensile behaviors are uniform as the low flow stress is accompanied by small generalized stability. In this context, the present work explains the experimental results[73-75,85,86] that alloying Cu, Mg and Si solutes with FCC-Al improves the strength and ductility of the according Al alloys. With this respect, Lee *et al.* experimentally found that adding small amounts of Mg solutes in FCC-Al results in Al-Mg alloys with both high strength and large ductility compared with pure Al[85]. The underlying mechanism can further be understood from variations in the SFE[87,88]. The first-principle calculations on composition-dependent three-dimensional misfit potentials[36] indicated the addition of Mg, Cu and Si solutes can decrease the intrinsic SFE values of Al alloys. In principle, the magnitude of SFE values determines the ease with the cross-slip of screw dislocations that occurs in Al alloys[89]. The reduced SFE can promote grain refinement and restrict dynamic recovery, favoring the formation of high-density stacking faults[85,90], which are beneficial to both strength and ductility. Due to the large SFE of FCC Al (~119.6 mJ/m^2), the partial dislocations that move under shear stress can easily recombine to form the full dislocations, facilitating the cross-slip of dislocations[36]. The SFE is reduced by increasing the Mg solute in FCC-Al[36], suggesting that the solute Mg in FCC Al makes the cross-slip more difficult to occur. The tangled dislocation structure leads to work hardening of the deformed region and the dispersion of deformation to the neighboring regions, thus reducing the strain localization degree and promoting spread-out deformation[85]. Thus, the Mg solute in FCC-Al can accommodate plastic strain via the dispersion of deformation in the alloy. Due to the lower SFE of Al-Mg alloys than that of FCC-Al, the partial dislocations can be widely spaced in Al-Mg alloys with increasing Mg contents. Consequently, the recombination of partial dislocations becomes more difficult, restricting the

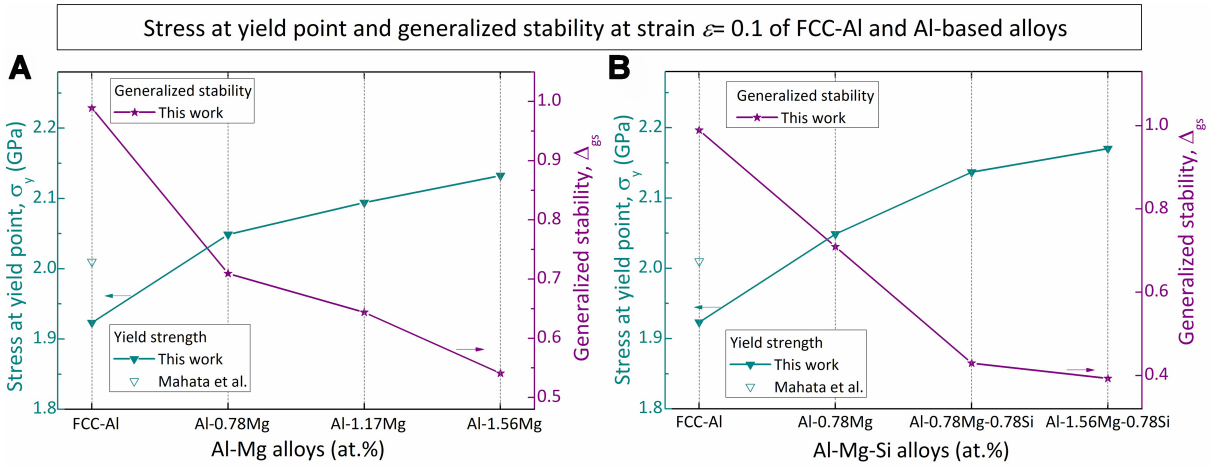

Figure 4. Yield stress and generalized stability upon tensile deformation of the FCC-Al and Al alloys. The stress at yield point and the generalized stability at strain of ε = 0.1 derived from the driving force and energy barrier for dislocation motion during tensile deformation of (A) binary Al-Mg alloys with different Mg solute contents and (B) ternary Al-Mg-Si alloys with different solutes Mg and Si contents, respectively. Note that the results calculated in this work are denoted by the solid point and the value referred from the literature[82] by the hollow point.

occurrence of dislocation cross-slip. These dislocations tend to move along the slip planes and form tangled dislocations along with dislocation band structure, which enhances the dislocation storage capacity and improves the strain-hardening effects[85]. The according manifestation is a high work hardening degree during plastic flow and reduced tendency for strain localization, which results in the high-strength Al-Mg alloys also exhibiting good ductility.

The distribution and evolution of mobile dislocations in the Al alloys with different solutes Mg and Si contents is shown in Figure 5, where the different lines represent multiple types of dislocations, including the <110>/2, <112>/6, and other dislocations marked by blue, green and red lines, respectively. The results indicate that the dislocations in alloy systems are initially activated at the yield point. With deformation proceedings, the dislocation behaviors become complex, which are accompanied by dislocation entanglement and dislocation reactions such as dislocation decomposition or synthesis. The interactions between these solutes and dislocations raise the complexity of irreversible deformation due to increased Mg and Si solutes in the alloy systems, which exert influences on the competition between dislocation storage and dislocation annihilation. As reflected in Figure 5B(i)-D(i), the full dislocation (denoted by the blue lines) with Burgers vector of <110>/2 is decomposed into two partial dislocations (denoted by the green lines) with Burgers vector of <112>/6, or the reverse dislocation reaction occurs during the irreversible deformation. The result is consistent with that predicted from the classical Peierls-Nabarro model for the FCC-Al and Al-based alloys[36,91].

Such dislocation reactions and defects interactions can generate sources for mobile dislocations, while the dislocation exhaustion occurs after the mobile dislocations move over a mean-free path. Due to distinctions in dislocation structure, formation energetics and immobility, the different types of dislocations and their interactions contribute differently to the strain-hardening effects[92]. The varied degree of Shockley partial dislocations (the green line shown in Figure 5) in these Al alloys with respect to their SFE exert different influences on the mechanical behaviors. Besides, more dislocation nucleation is associated with higher driving force for dislocation motion and faster rate for dislocation evolution. In this context, initiating new dislocation is more difficult than the primitive one, resulting in the small generalized stability and/or

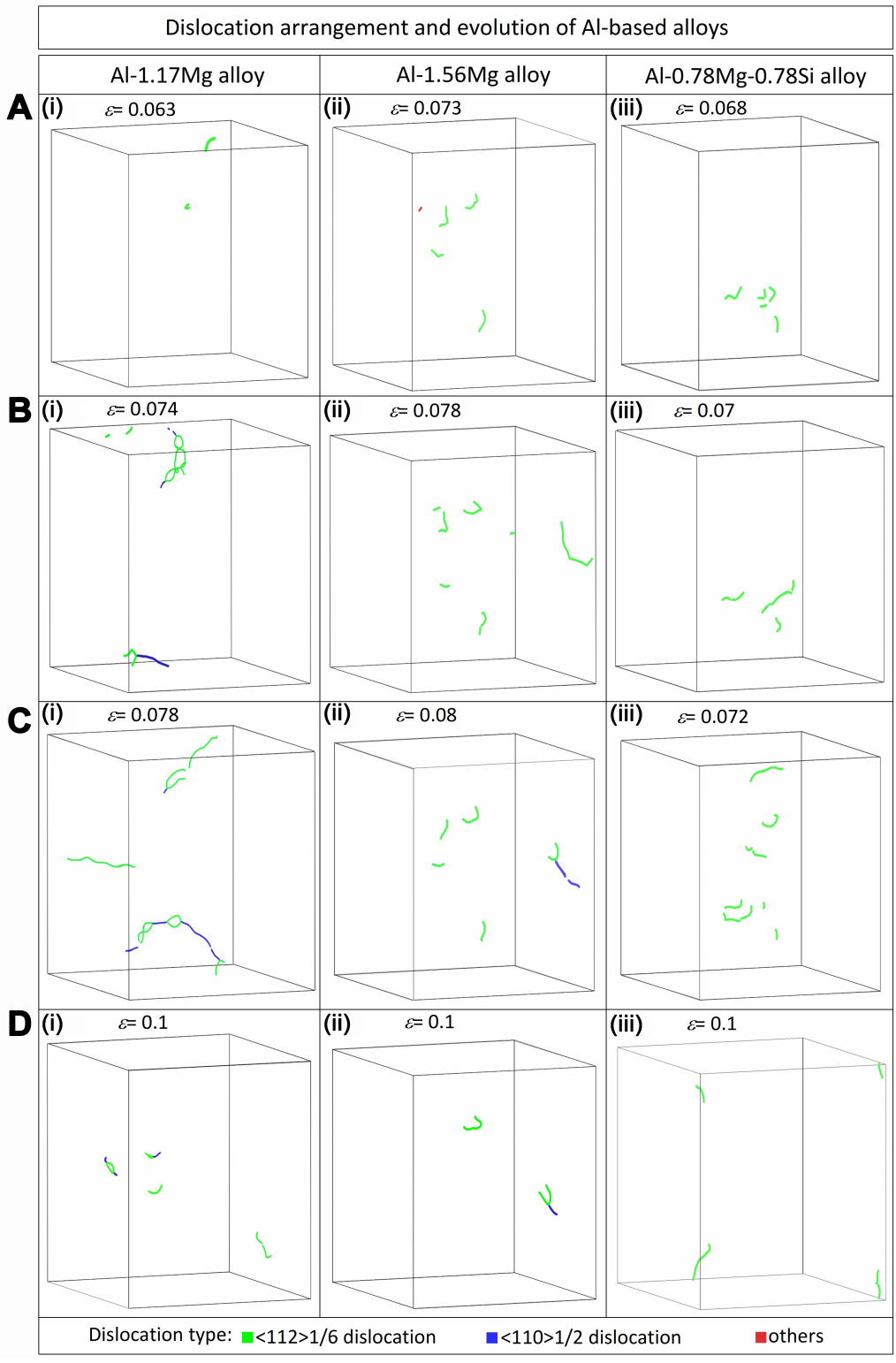

Figure 5. Dislocation arrangement and evolution of Al alloys with additional Mg and Si solutes. Snapshots of the mobile dislocation distribution of [A(i)-D(i)] the Al-1.17Mg alloy, [A(ii)-D(ii)] the Al-1.56Mg alloy, and [A(iii)-D(iii)] the Al-0.78Mg-0.78Si alloy at different magnitudes of strain during tensile deformation, respectively.

thermo-kinetic partition. The primary dislocations in Al-Mg and Al-Mg-Si alloys upon irreversible deformation are the Shockley partial dislocations represented by the green lines in Figure 5. This indicates that the deformation is dominated by partial dislocations of these Al alloys, which agrees well with the previous results[91,93].

Prospect of current thermo-kinetic models in designing higher-performing alloys

It is worth noting that the present work focuses on dilute alloys, where the solute contents are lower than the maximum solid solubility[36,94]. Once the amount of additional solutes in the α-Al matrix is over the maximum solubility, precipitation will occur and different kinds of precipitates will form in Al alloys. For instance, when the solutes Mg and Si contents are over their maximum solubility, the precipitates including the solute clusters, β' and β'' phases will form in the Al-Mg-Si alloys[45,95]. These precipitates exert interactions with dislocations in the alloy system, thus influencing the mechanical properties of the Al alloys. Within the present framework, the mechanical properties of these precipitation-strengthened Al alloys can be predicted via the theoretical models developed on the basis of the thermo-kinetic synergistic effects in Section "Materials and Methods". The precipitates and the interactions between dislocations and precipitates affect the dislocation evolution (i.e., the total dislocation density ρ_t and the mobile dislocation density ρ_m) upon deformation. These exert direct influences on the glide resistance and the effective separation of dislocation slip, which is finally reflected in the variations of thermo-kinetic partition and generalized stability.

Upon deformation, the system energy accumulated by dislocation nucleation is mostly dissipated by dislocation motion. In principle, a more sustainable work hardening (or work softening) stage can be obtained by adjusting a slower speed for system energy accumulation (or dissipation)[96,97]. As such, the variation in activation volume or thermo-kinetic partition for microstructure deformation derives from that for microstructure formation in terms of phase transition. Hence, acquiring an ideal deformation mode by designing the activation volume or thermo-kinetic partition in terms of alloy composition and processing parameters becomes the central point to obtain an ideal match between strength and ductility of Al alloys. With a sufficiently sustainable process of dislocation motion, the primitive thermo-kinetic partition can be changed to obtain a more persistent work hardening process, which requires high applied stress as the driving force for dislocation evolution. Thus, the mechanical performance paradox with respect to a primitive work hardening mode[79-81] can be modified in terms of an enhanced activation volume or thermo-kinetic partition, which corresponds to an ideal thermo-kinetic synergy, as schematically illustrated in Figure 6. Therefore, the critical point for designing an ideal strength-ductility match lies in obtaining a high strain hardening capability by making the dislocation initiation more difficult to occur and the propagation of dislocation more persistent. As such, following the thermo-kinetic synergy upon materials processing, the prediction for mechanical performances directly from composition/processing and the inverse design for composition/processing of advanced Al-based alloys with good comprehensive mechanical performance can be achieved. Our continuous investigations in this direction are still underway, the results of which will be reported in the near future.

CONCLUSIONS

In summary, the physical origins behind the strength-ductility paradox of aluminum alloys were investigated from the thermo-kinetic synergy in combination with the MD simulations. Following the classical dislocation theories and strengthening/toughening mechanisms, the theoretical models for quantitative connections among yield strength, plastic strain and dislocation density are established in terms of the driving force and energy barrier. It turns out that the thermo-kinetic synergy upon materials processing is responsible for mechanical performance paradox. The yield strength (plastic strain) and

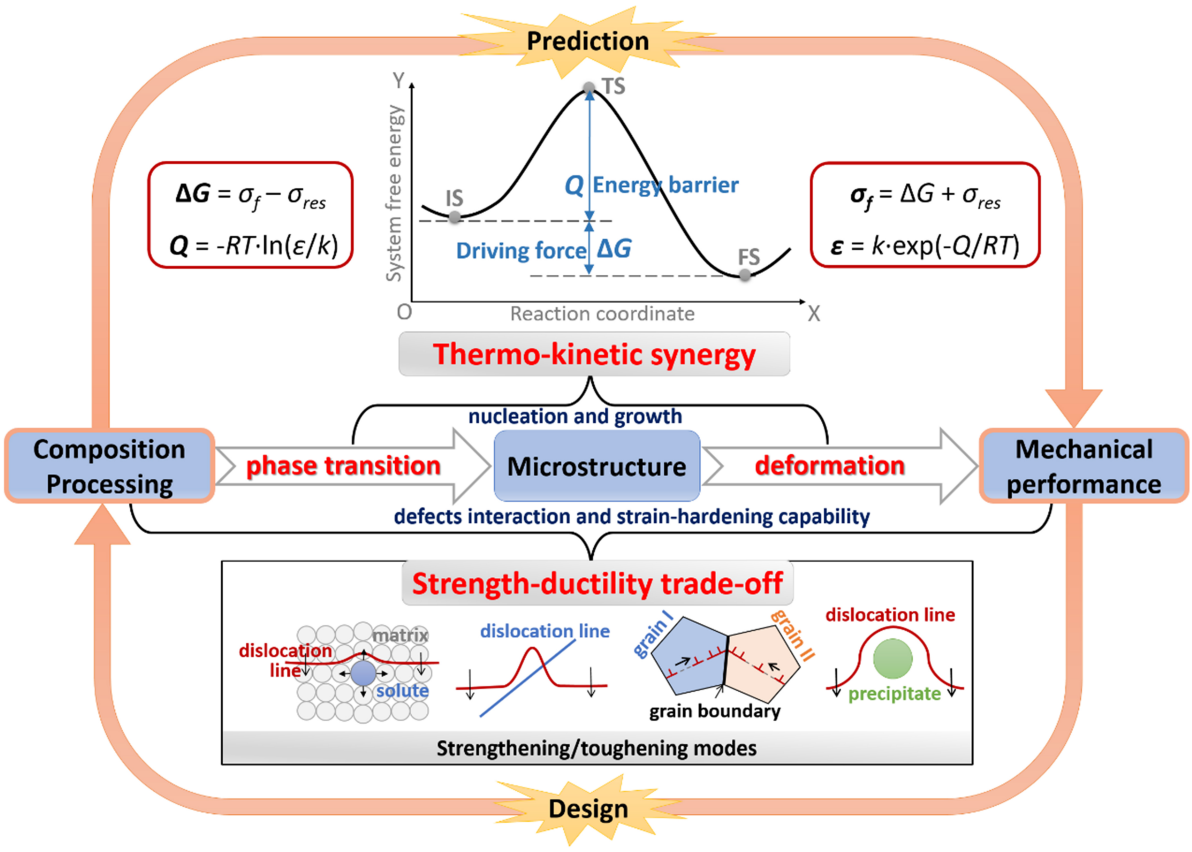

Figure 6. Schematic illustration of prediction for the mechanical performances from composition/processing, or the inverse design of the composition/processing for Al alloys with desired mechanical performances, based on the thermo-kinetic synergistic effects of phase transition and deformation bridged by the microstructure in terms of the defects interactions with respect to the classical strengthening/toughening modes (including the solid solution hardening, the dislocation hardening, the phase/grain boundary hardening, and the precipitation hardening modes), the quantitative correlations between strength (σ) and ductility (ε) along with thermodynamic driving force (ΔG) and kinetic energy barrier (Q), as denoted in the reaction coordinate diagram with respect to the initial state (IS), the transition state (TS) and the final state (FS) of alloy system during phase transition and/or deformation, respectively.

driving force (energy barrier) for dislocation motion behave in positive correlations. These quantitative models are validated in FCC-Al and Al alloys with Mg, Cu and Si solutes. The tensile performances and dislocation behaviors of these Al alloys are analyzed to determine the generalized stability with respect to the driving force and energy barrier in terms of dislocation density. Compared with FCC-Al, a typical thermo-kinetic partition of large driving force and small generalized stability presents for the Al alloys with Mg, Cu and Si solutes, which explains the very reason behind different combinations of strength and ductility of these alloys. The present work provides an insightful thermo-kinetic guideline to understand the exclusive behaviors of strength and ductility of metallic alloys. By making the dislocation initiation more difficult and the propagation of dislocation more persistent to achieve a high strain hardening capability, advanced Al alloys with an ideal strength-ductility match can be designed by adjusting the thermo-kinetic partition or activation volume in terms of the composition/processing dependent driving force and energy barrier.

DECLARATIONS

Authors' contributions

Conceptualization, supervision: Du, J.; Liu, F.

Investigation, writing original draft: Du, J.; Liu, Y.; Zhao, C.
Writing review and editing: Du, J.; Song, K.; Liu, F.
Investigation, methodology, data curation, discussion: Du, J.; Liu, Y.; Zhao, C.; Xue, H.; Gao, K.; Fang, X.
Funding acquisition: Du, J.; Liu, F.

Availability of data and materials

The data that support the findings of this study are available from the corresponding author upon reasonable request.

Financial support and sponsorship

This work is financially supported by the National Natural Science Foundation of China (Grant Nos. 52171013 and 52130110), the Natural Science Foundation of Chongqing (Grant No. CSTB2022NSCQ-MSX0369), the Research Fund of the State Key Laboratory of Solidification Processing (NPU) China (Grant No. 2023-QZ-03), and the "2020-2022 Youth Talent Promotion Project" of China Association for Science and Technology (Grant No. 2020QNRC001). The authors acknowledge the Analytical & Testing Center and the High-Performance Computing Center of NPU for access to supercomputing facilities.

Conflicts of interest

All authors declared that there are no conflicts of interest.

Ethical approval and consent to participate

Not applicable.

Consent for publication

Not applicable.

REFERENCES

1. Chen, J. H.; Costan, E.; van, H. M. A.; Xu, Q.; Zandbergen, H. W. Atomic pillar-based nanoprecipitates strengthen AlMgSi alloys. *Science* **2006**, *312*, 416-9. DOI PubMed
2. Zhang, J.; Zhou, D.; Pang, X.; et al. Deformation-induced concurrent formation of 9R phase and twins in a nanograined aluminum alloy. *Acta. Mater.* **2023**, *244*, 118540. DOI
3. Raabe, D.; Ponge, D.; Uggowitzer, P. J.; et al. Making sustainable aluminum by recycling scrap: the science of "dirty" alloys. *Prog. Mater. Sci.* **2022**, *128*, 100947. DOI
4. Liddicoat, P. V.; Liao, X. Z.; Zhao, Y.; et al. Nanostructural hierarchy increases the strength of aluminium alloys. *Nat. Commun.* **2010**, *1*, 63. DOI
5. Costa Teixeira J, Cram D, Bourgeois L, Bastow T, Hill A, Hutchinson C. On the strengthening response of aluminum alloys containing shear-resistant plate-shaped precipitates. *Acta. Mater.* **2008**, *56*, 6109-22. DOI
6. Simar, A.; Bréchet, Y.; de, M. B.; Denquin, A.; Pardoen, T. Sequential modeling of local precipitation, strength and strain hardening in friction stir welds of an aluminum alloy 6005A-T6. *Acta. Mater.* **2007**, *55*, 6133-43. DOI
7. Ogura, T.; Otani, T.; Hirose, A.; Sato, T. Improvement of strength and ductility of an Al–Zn–Mg alloy by controlling grain size and precipitate microstructure with Mn and Ag addition. *Mater. Sci. Eng. A.* **2013**, *580*, 288-93. DOI
8. Macías JG, Douillard T, Zhao L, Maire E, Pyka G, Simar A. Influence on microstructure, strength and ductility of build platform temperature during laser powder bed fusion of AlSi10Mg. *Acta. Mater.* **2020**, *201*, 231-43. DOI
9. Chen, X.; Guo, M.; Du, J.; Zhuang, L. Synergistic mechanism of hetero-structured Al–Mg–Si–Cu–Zn–Fe–Mn alloys with greatly enhanced strength, ductility and formability. *Mater. Sci. Eng. A.* **2024**, *910*, 146893. DOI
10. Ma, E.; Wu, X. Tailoring heterogeneities in high-entropy alloys to promote strength-ductility synergy. *Nat. Commun.* **2019**, *10*, 5623. DOI PubMed PMC
11. Ma, E.; Zhu, T. Towards strength–ductility synergy through the design of heterogeneous nanostructures in metals. *Mater. Today.* **2017**, *20*, 323-31. DOI

12. Du, J.; Liu, Y.; Zhang, Z.; et al. Mechanical behaviors of metallic alloys dominated by thermo-kinetic synergistic effects upon materials processing. *Mater. Today. Commun.* **2023**, *37*, 107218. DOI
13. Hu, X.; Zhao, J.; Chen, Y.; et al. Structure-property modeling scheme based on optimized microstructural information by two-point statistics and principal component analysis. *J. Mater. Inf.* **2022**, *2*, 5. DOI
14. Wang, W. Y.; Yin, J.; Chai, Z.; et al. Big data-assisted digital twins for the smart design and manufacturing of advanced materials: from atoms to products. *J. Mater. Inf.* **2022**, *2*, 1. DOI
15. Fan, L.; Yang, T.; Zhao, Y.; et al. Ultrahigh strength and ductility in newly developed materials with coherent nanolamellar architectures. *Nat. Commun.* **2020**, *11*, 6240. DOI PubMed PMC
16. Wang, F.; Li, Y.; Chen, X.; et al. Superior strength–ductility combination in Al alloys via dislocation gradient structure. *Mater. Res. Lett.* **2023**, *11*, 347-53. DOI
17. Lu, Q.; Li, K.; Chen, H.; et al. Simultaneously enhanced strength and ductility of 6xxx Al alloys via manipulating meso-scale and nano-scale structures guided with phase equilibrium. *J. Mater. Sci. Technol.* **2020**, *41*, 139-48. DOI
18. Du, J.; Zhang, A.; Zhang, Y.; Wang, T.; Xiong, S.; Liu, F. Atomistic determination on stability, cluster and microstructures in terms of crystallographic and thermo-kinetic integration of Al−Mg−Si alloys. *Mater. Today. Commun.* **2020**, *24*, 101220. DOI
19. Du, J.; Wen, B. Composition-structure-property correlations of complex metallic alloys described by the “cluster-plus-glue-atom” model. *Appl. Mater. Today.* **2017**, *7*, 13-46. DOI
20. Leyson, G.; Hector, L.; Curtin, W. Solute strengthening from first principles and application to aluminum alloys. *Acta. Mater.* **2012**, *60*, 3873-84. DOI
21. Shercliff, H.; Ashby, M. A process model for age hardening of aluminium alloys - II. Applications of the model. *Acta. Metall. Mater.* **1990**, *38*, 1803-12. DOI
22. Sun, W.; Zhu, Y.; Marceau, R.; et al. Precipitation strengthening of aluminum alloys by room-temperature cyclic plasticity. *Science* **2019**, *363*, 972-5. DOI
23. Liu, G.; Sun, J.; Nan, C.; Chen, K. Experiment and multiscale modeling of the coupled influence of constituents and precipitates on the ductile fracture of heat-treatable aluminum alloys. *Acta. Mater.* **2005**, *53*, 3459-68. DOI
24. Du, J.; Wen, B.; Melnik, R.; Kawazoe, Y. Cluster characteristics and physical properties of binary Al–Zr intermetallic compounds from first principles studies. *Comput. Mater. Sci.* **2015**, *103*, 170-8. DOI
25. Du, J.; Zhang, A.; Zhang, L.; Xiong, S.; Liu, F. Quantitative and qualitative correlations by atomistic determination for the precipitated phases in Al–Li–Cu system. *Intermetallics* **2019**, *112*, 106551. DOI
26. Bardel, D.; Perez, M.; Nelias, D.; et al. Coupled precipitation and yield strength modelling for non-isothermal treatments of a 6061 aluminium alloy. *Acta. Mater.* **2014**, *62*, 129-40. DOI
27. Vannarat, S.; Sluiter, M. H. F.; Kawazoe, Y. First-principles study of solute-dislocation interaction in aluminum-rich alloys. *Phys. Rev. B.* **2001**, *64*, 224203. DOI
28. Zhang, X.; Lu, S.; Zhang, B.; Tian, X.; Kan, Q.; Kang, G. Dislocation–grain boundary interaction-based discrete dislocation dynamics modeling and its application to bicrystals with different misorientations. *Acta. Mater.* **2021**, *202*, 88-98. DOI
29. Gorbatov, O.; Stroev, A.; Gornostyrev, Y.; Korzhavyi, P. Effective cluster interactions and pre–precipitate morphology in binary Al-based alloys. *Acta. Mater.* **2019**, *179*, 70-84. DOI
30. Bignon, M.; Ma, Z.; Robson, J. D.; Shanthraj, P. Interactions between plastic deformation and precipitation in aluminium alloys: a crystal plasticity model. *Acta. Mater.* **2023**, *247*, 118735. DOI
31. Krasnikov, V.; Mayer, A.; Pogorelko, V.; Latypov, F.; Ebel, A. Interaction of dislocation with GP zones or θ" phase precipitates in aluminum: atomistic simulations and dislocation dynamics. *Int. J. Plast.* **2020**, *125*, 169-90. DOI
32. Niewczas, M.; Jobba, M.; Mishra, R. Thermally activated flow of dislocations in Al–Mg binary alloys. *Acta. Mater.* **2015**, *83*, 372-82. DOI
33. Fan, H.; Wang, Q.; El-Awady, J. A.; Raabe, D.; Zaiser, M. Strain rate dependency of dislocation plasticity. *Nat. Commun.* **2021**, *12*, 1845. DOI PubMed PMC
34. Chen, M.; Ma, E.; Hemker, K. J.; Sheng, H.; Wang, Y.; Cheng, X. Deformation twinning in nanocrystalline aluminum. *Science* **2003**, *300*, 1275-7. DOI
35. Mahajan, S.; Chin, G. Formation of deformation twins in f.c.c. crystals. *Acta. Metall.* **1973**, *21*, 1353-63. DOI
36. Du, J.; Liu, Y.; Zhang, Z.; et al. Deformation behaviors in light of dislocation core characteristics with respect to the compositional-dependent misfit potentials of aluminum alloys. *J. Mater. Res. Technol.* **2023**, *27*, 4366-77. DOI
37. Liu, F. Nucleation/growth design by thermo-kinetic partition. *J. Mater. Sci. Technol.* **2023**, *155*, 72-81. DOI
38. He, Y.; Song, S.; Du, J.; et al. Thermo-kinetic connectivity by integrating thermo-kinetic correlation and generalized stability. *J. Mater. Sci. Technol.* **2022**, *127*, 225-35. DOI
39. Huang, L.; Lin, W.; Zhang, Y.; et al. Generalized stability criterion for exploiting optimized mechanical properties by a general correlation between phase transformations and plastic deformations. *Acta. Mater.* **2020**, *201*, 167-81. DOI
40. Wang, T.; Liu, F. Multiscale thermo-kinetic characterization for β′ and β1 precipitation in Mg-Sm alloys. *Acta. Mater.* **2023**, *254*, 119011. DOI
41. Wang, T.; Liu, F. Optimizing mechanical properties of magnesium alloys by philosophy of thermo-kinetic synergy: review and outlook. *J. Magnes. Alloys.* **2022**, *10*, 326-55. DOI
42. Zhang, Y.; Song, S.; Liu, F. Thermo-kinetic orientation study on interface behavior of polycrystalline Cu-Nb composite by crystal

plasticity finite element method. *Mater. Design.* **2022**, *223*, 111215. DOI
43. Liu, Y.; Du, J.; Shang, S.; et al. Insights into plastic deformation mechanisms of austenitic steels by coupling generalized stacking fault energy and semi-discrete variational Peierls-Nabarro model. *Prog. Nat. Sci. Mater. Int.* **2023**, *33*, 83-91. DOI
44. Zhang, Y.; Du, J.; Wang, K.; Wang, H.; Li, S.; Liu, F. Application of non-equilibrium dendrite growth model considering thermo-kinetic correlation in twin-roll casting. *J. Mater. Sci. Technol.* **2020**, *44*, 209-22. DOI
45. Du, J.; Zhang, Z.; Liu, Y.; et al. Strength-ductility trade-off modulated by thermo-kinetic synergy of heat-treatable aluminum alloys. *J. Mater. Res. Technol.* **2023**, *24*, 7876-95. DOI
46. Liu, Y.; Du, J.; Zhang, K.; et al. Orientation-dependent mechanical behaviors of BCC-Fe in light of the thermo-kinetic synergy of plastic deformation. *Materials* **2024**, *17*, 2395. DOI PubMed PMC
47. Chen, H.; Chen, Z.; Ji, G.; et al. Experimental and modelling assessment of ductility in a precipitation hardening AlMgScZr alloy. *Int. J. Plast.* **2021**, *139*, 102971. DOI
48. Yang, M.; Orekhov, A.; Hu, Z.; et al. Shearing and rotation of β″ and β′ precipitates in an Al-Mg-Si alloy under tensile deformation: in-situ and ex-situ studies. *Acta. Mater.* **2021**, *220*, 117310. DOI
49. Kocks, U. F.; Argon, A. S.; Ashby, M. F. Thermodynamics and kinetics of slip. 1975. https://api.semanticscholar.org/CorpusID:137701656. (accessed 2025-02-11).
50. Argon, A. Strengthening mechanisms in crystal plasticity. Oxford University Press, 2008. DOI
51. Cheng, L. M.; Poole, W. J.; Embury, J. D.; Lloyd, D. J. The influence of precipitation on the work-hardening behavior of the aluminum alloys AA6111 and AA7030. *Metall. Mater. Trans. A.* **2003**, *34*, 2473-81. DOI
52. Myhr, O. R.; Grong, Ø.; Andersen, S. J. Modelling of the age hardening behaviour of Al–Mg–Si alloys. *Acta. Mater.* **2001**, *49*, 65-75. DOI
53. Hansen, N. Hall–Petch relation and boundary strengthening. *Scr. Mater.* **2004**, *51*, 801-6. DOI
54. Esmaeili, S.; Lloyd, D.; Poole, W. A yield strength model for the Al-Mg-Si-Cu alloy AA6111. *Acta. Mater.* **2003**, *51*, 2243-57. DOI
55. Arsenlis, A.; Parks, D. M. Modeling the evolution of crystallographic dislocation density in crystal plasticity. *J. Mech. Phys. Solids.* **2002**, *50*, 1979-2009. DOI
56. Orowan, E. Problems of plastic gliding. *Proc. Phys. Soc.* **1940**, *52*, 8-22. DOI
57. Pan, B.; Shibutani, Y.; Tanaka, H. Dislocation-based constitutive model of crystal plasticity for the size effect of single crystalline micropillar samples. *Mech. Eng. J.* **2016**, *3*, 15-00602. DOI
58. Caillard, D.; Martin, J. L. Chapter 8 - Dislocation climb. In: Thermally activated mechanisms in crystal plasticity. Amsterdam: Elsevier. 2003;8:281-319. DOI
59. Wang, S.; Hashimoto, N.; Wang, Y.; Ohnuki, S. Activation volume and density of mobile dislocations in hydrogen-charged iron. *Acta. Mater.* **2013**, *61*, 4734-42. DOI
60. Plimpton, S. Fast parallel algorithms for short-range molecular dynamics. *J. Comput. Phys.* **1995**, *117*, 1-19. DOI
61. Jelinek, B.; Groh, S.; Horstemeyer, M. F.; et al. Modified embedded atom method potential for Al, Si, Mg, Cu, and Fe alloys. *Phys. Rev. B.* **2012**, *85*, 245102. DOI
62. Hue DT, Tran V, Nguyen V, Van Lich L, Dinh V, Nguyen T. High strain-rate effect on microstructure evolution and plasticity of aluminum 5052 alloy nano-multilayer: a molecular dynamics study. *Vacuum* **2022**, *201*, 111104. DOI
63. Zhang, L.; Shibuta, Y.; Huang, X.; Lu, C.; Liu, M. Grain boundary induced deformation mechanisms in nanocrystalline Al by molecular dynamics simulation: from interatomic potential perspective. *Comput. Mater. Sci.* **2019**, *156*, 421-33. DOI
64. Xu, Y.; Wang, M.; Zhu, F.; et al. A molecular dynamic study of nano-grinding of a monocrystalline copper-silicon substrate. *Appl. Surf. Sci.* **2019**, *493*, 933-47. DOI
65. Fan, H.; El-awady, J. A. Towards resolving the anonymity of pyramidal slip in magnesium. *Mater. Sci. Eng. A.* **2015**, *644*, 318-24. DOI
66. Xing, Z.; Fan, H.; Tang, J.; Wang, B.; Kang, G. Molecular dynamics simulation on the cyclic deformation of magnesium single crystals. *Comput. Mater. Sci.* **2021**, *186*, 110003. DOI
67. Sun, X.; Fan, S.; Peng, M.; et al. Classical molecular dynamics simulation of atomic structure transitions in FeSiCuMgAl high-entropy alloys under biaxial stretching. *Mater. Today. Commun.* **2024**, *40*, 109716. DOI
68. Husain, A.; La, P.; Hongzheng, Y.; Jie, S. Molecular dynamics as a means to investigate grain size and strain rate effect on plastic deformation of 316 L nanocrystalline stainless-steel. *Materials* **2020**, *13*, 3223. DOI PubMed PMC
69. Sainath, G.; Choudhary, B. Orientation dependent deformation behaviour of BCC iron nanowires. *Comput. Mater. Sci.* **2016**, *111*, 406-15. DOI
70. Stukowski, A. Visualization and analysis of atomistic simulation data with OVITO - the Open Visualization Tool. *Modell. Simul. Mater. Sci. Eng.* **2010**, *18*, 015012. DOI
71. Stukowski, A.; Bulatov, V. V.; Arsenlis, A. Automated identification and indexing of dislocations in crystal interfaces. *Modell. Simul. Mater. Sci. Eng.* **2012**, *20*, 085007. DOI
72. Sendrowicz, A.; Myhre, A.; Yasnikov, I.; Vinogradov, A. Stored and dissipated energy of plastic deformation revisited from the viewpoint of dislocation kinetics modelling approach. *Acta. Mater.* **2022**, *237*, 118190. DOI
73. Li, Z.; Zhao, P.; Jia, Z.; Liu, Z.; Xie, Z. Effects of Mg and Si contents on the microstructure and mechanical properties of AA6014 alloys in T4P and T6P temper. *Mater. Sci. Eng. A.* **2019**, *740-1*, 187-200. DOI
74. Khangholi, S. N.; Javidani, M.; Maltais, A.; Chen, X. Effect of Ag and Cu addition on the strength and electrical conductivity of Al-

Mg-Si alloys using conventional and modified thermomechanical treatments. *J. Alloys. Compd.* **2022**, *914*, 165242. DOI

75. Zhu, L.; Guo, M.; Zhang, J. Effect of silicon content on nucleation and growth of multiscale precipitates in Al–Mg–Si–Cu–Zn alloys for different aging paths. *Mater. Sci. Eng. A.* **2022**, *841*, 143016. DOI
76. Zepeda-Ruiz, L. A.; Stukowski, A.; Oppelstrup, T.; Bulatov, V. V. Probing the limits of metal plasticity with molecular dynamics simulations. *Nature* **2017**, *550*, 492-5. DOI PubMed
77. Wei, Y.; Bower, A. F.; Gao, H. Enhanced strain-rate sensitivity in fcc nanocrystals due to grain-boundary diffusion and sliding. *Acta. Mater.* **2008**, *56*, 1741-52. DOI
78. Ma, K.; Wen, H.; Hu, T.; et al. Mechanical behavior and strengthening mechanisms in ultrafine grain precipitation-strengthened aluminum alloy. *Acta. Mater.* **2014**, *62*, 141-55. DOI
79. Kamikawa, N.; Huang, X.; Tsuji, N.; Hansen, N. Strengthening mechanisms in nanostructured high-purity aluminium deformed to high strain and annealed. *Acta. Mater.* **2009**, *57*, 4198-208. DOI
80. Frigaard, Ø.; Grong, Ø.; Midling, O. T. A process model for friction stir welding of age hardening aluminum alloys. *Metall. Mater. Trans. A.* **2001**, *32*, 1189-200. DOI
81. Starink, M.; Deschamps, A.; Wang, S. The strength of friction stir welded and friction stir processed aluminium alloys. *Scr. Mater.* **2008**, *58*, 377-82. DOI
82. Mahata, A.; Asle, Z. M. Evolution of solidification defects in deformation of nano-polycrystalline aluminum. *Comput. Mater. Sci.* **2019**, *163*, 176-85. DOI
83. Kadau, K.; Lomdahl, P. S.; Holian, B. L.; et al. Molecular-dynamics study of mechanical deformation in nano-crystalline aluminum. *Metall. Mater. Trans. A.* **2004**, *35*, 2719-23. DOI
84. Hocker, S.; Hummel, M.; Binkele, P.; Lipp, H.; Schmauder, S. Molecular dynamics simulations of tensile tests of Ni-, Cu-, Mg- and Ti-alloyed aluminium nanopolycrystals. *Comput. Mater. Sci.* **2016**, *116*, 32-43. DOI
85. Lee, B.; Kim, S.; Park, J.; Kim, H.; Lee, J. Role of Mg in simultaneously improving the strength and ductility of Al–Mg alloys. *Mater. Sci. Eng. A.* **2016**, *657*, 115-22. DOI
86. Remøe, M. S.; Marthinsen, K.; Westermann, I.; Pedersen, K.; Røyset, J.; Marioara, C. The effect of alloying elements on the ductility of Al-Mg-Si alloys. *Mater. Sci. Eng. A.* **2017**, *693*, 60-72. DOI
87. Matsuda, K.; Teguri, D.; Sato, T.; Uetani, Y.; Ikeno, S. Cu segregation around metastable phase in Al-Mg-Si alloy with Cu. *Mater. Trans.* **2007**, *48*, 967-74. DOI
88. Tian, Y.; Shibata, A.; Zhang, Z.; Tsuji, N. Ductility sensitivity to stacking fault energy and grain size in Cu–Al alloys. *Mater. Res. Lett.* **2016**, *4*, 112-7. DOI
89. Van Swygenhoven, H.; Derlet, P. M.; Frøseth, A. G. Stacking fault energies and slip in nanocrystalline metals. *Nat. Mater.* **2004**, *3*, 399-403. DOI PubMed
90. An, X.; Wu, S.; Zhang, Z.; Figueiredo, R.; Gao, N.; Langdon, T. Enhanced strength–ductility synergy in nanostructured Cu and Cu–Al alloys processed by high-pressure torsion and subsequent annealing. *Scr. Mater.* **2012**, *66*, 227-30. DOI
91. Vitek, V. Atomic level computer modelling of crystal defects with emphasis on dislocations: past, present and future. *Prog. Mater. Sci.* **2011**, *56*, 577-85. DOI
92. Bajaj, D.; Chen, D. Uncovering all possible dislocation locks in face-centered cubic materials. *Int. Jo. Plast.* **2024**, *181*, 104101. DOI
93. Su, R.; Neffati, D.; Xue, S.; et al. Deformation mechanisms in FCC Co dominated by high-density stacking faults. *Mater. Sci. Eng. A.* **2018**, *736*, 12-21. DOI
94. Takeuchi, A.; Inoue, A. Classification of bulk metallic glasses by atomic size difference, heat of mixing and period of constituent elements and its application to characterization of the main alloying element. *Mater. Trans.* **2005**, *46*, 2817-29. DOI
95. Zhang, Z.; Du, J.; Zhang, K.; Yang, X.; Song, K.; Liu, F. An aging processing design scheme derived from precipitation thermo-kinetic synergy of heat-treatable aluminum alloys. *Mater. Sci. Eng. A.* **2025**, *919*, 147505. DOI
96. Seeger, A.; Diehl, J.; Mader, S.; Rebstock, H. Work-hardening and work-softening of face-centred cubic metal crystals. *Philos. Mag.* **1957**, *2*, 323-50. DOI
97. Yang, C.; Pan, J.; Lee, T. Work-softening and anneal-hardening behaviors in fine-grained Zn–Al alloys. *J. Alloys. Compd.* **2009**, *468*, 230-6. DOI
98. Devaney, R. J.; Barrett, R. A.; O'donoghue, P. E.; Leen, S. B. A dislocation mechanics constitutive model for effects of welding-induced microstructural transformation on cyclic plasticity and low-cycle fatigue for X100Q bainitic steel. *Int. J. Fatigue.* **2021**, *145*, 106097. DOI